

Selection rules for quasiparticle interference with internal nonsymmorphic symmetries

Raquel Queiroz^{1,*} and Ady Stern^{1,†}

¹*Department of Condensed Matter Physics, Weizmann Institute of Science, Rehovot 7610001, Israel*

(Dated: December 11, 2018)

We study how nonsymmorphic symmetries that commute with lattice translations are reflected in the quasiparticle interference (QPI) maps measured by scanning tunneling microscopy (STM). QPI maps, which result from scattering of Bloch states off impurities, record the interference of incoming and scattered waves as a function of energy and tip's position. Although both the impurity and the tip generically break spatial symmetries, we find that the QPI maps provide universal information on these symmetries. The symmetries impose constraints on the relation between various momentum components of the Bloch functions. These relations result in selection rules on certain momentum transfers in QPI maps. We find that universal information is encoded in the absence of QPI signal, or in the relative intensity of its replications. We show examples for one-dimensional chains and an effective model of the layered compound ZrSiS. We discuss the implications of our theory in the analysis of observed QPI of the Weyl semimetal TaAs. Our theory is particularly relevant for materials in rod and layer space groups, or when a correlated order parameter, such as antiferromagnetism, enlarges the unit cell.

Introduction — Symmetry plays a pivotal role in band theory for the determination of the global features of energy bands, even in the absence of details of the microscopic Hamiltonian [1–5]. The block diagonalization of the Hilbert space by symmetry representations can lead to stable or enforced band crossings in the Brillouin zone (BZ) [6–11]. These realize exotic relativistic fermions on the lattice that dominate transport properties when close to the Fermi level [12] and are currently the target of active research. To verify their stability, a direct experimental inspection of the symmetry character of Bloch electrons is of unquestioned value, but it is not an easy task. It is notably challenging when the symmetries are nonsymmorphic. These are unique to crystalline environments, combining a point-group action with fractional lattice translations. Direct experimental probes, such as tunneling or photoemission spectroscopy, couple either to momentum (\hat{p}) or position (\hat{r}) eigenvalues and therefore cannot preserve nonsymmorphic symmetries. One would naively think that consequently their eigenvalues cannot be measured by these techniques. In this work, we see that this is indeed not true: There are precise symmetry signatures in the response to spectroscopic probes, which may be relevant for the measurement of crystalline topological materials, for example in Ref. [13].

Our strategy is to find universal, symmetry-enforced, selection rules in the interference pattern created by elastically scattered electrons due to dilute impurities. Fourier-transformed STM, or QPI [14–18], measures fluctuations of the density of states $N(r)$ through a differential conductance map around an isolated impurity. Through a Fourier transformation, it is possible to identify the contribution of elastic scattering events according to a fixed momentum transfer $N(q)$. The relative intensity of the differential conductance peaks depends on unknown details of the impurity and tunneling elements of the measuring tip, obscuring the interpretation of a QPI pattern. Here we offer an argument based solely on symmetry to extract information from relative peak intensities, remarkably evident in the presence of nonsymmorphic symmetries. Sim-

ply put,

$$N_{\nu'-\nu}(q) = 0, \quad \text{if } \omega^{(\nu'-\nu)+(\beta-\alpha)} \neq 1. \quad (1)$$

where ω is a phase that characterizes the unitary symmetry, whose eigenvalues at the Γ -point are ω^ν with ν an integer; α counts the number of times q crosses the BZ boundary along the direction of the fractional translation. QPI replications are labelled by different α along the nonsymmorphic direction. Finally, β is determined by the properties of the tunneling tip. Even though β is not generally fixed, a single measurement can strongly favor one.

Equation (1) gives us a necessary condition for a β -tip to observe QPI amplitude from a transition between two energy eigenstates with symmetry flavors ν and ν' through a momentum transfer of q , when q crosses the BZ boundary α times. In the following sections we prove this statement by expressing the eigenstates as a function of the local degrees of freedom, position \hat{r} and eigenstates of the point group \hat{R} , resolving how the symmetry is manifested when the system is coupled to a local tunneling tip \hat{M} . We find a decomposition of the energy eigenstates relating the Bloch component and the \hat{R} eigenvalue, leading to scattering selection rules that depend on q .

Eigenstates and internal symmetries — We restrict our study to cases where the symmetry operator commutes with lattice translations. This implies that it acts on a set of internal degrees of freedom, eigenvalues of a local operator \hat{O} . This operator labels the atomic orbitals, $\phi_o(r)$ by a quantum number o . It can refer to spin or any representation of the local point group. The form of $\phi_o(r)$ is determined by microscopic details of the Hamiltonian, but nevertheless highly constrained by the symmetries. An energy eigenstate is generally written as

$$|\psi_b^{\nu k}\rangle = \sum_o \int_r \phi_o^{\nu k, b}(r) |o; r\rangle, \quad (2)$$

where ν labels the symmetry eigenvalue, k the crystal momentum and b a band index, omitted in the following. The combined notation $|o; r\rangle \equiv |o\rangle \otimes |r\rangle$ stands for eigenstates

of both \hat{O} and \hat{r} , forming a basis that satisfies $\langle o; r|o'; r' \rangle = \delta_{oo'}\delta(r-r')$.

We consider a discrete transformation, say a rotation, that respects $\hat{R}^n = \hat{1}$. Its possible eigenvalues are given by the integer powers of $\omega = \exp\{2\pi i/n\}$, with matrix representation ρ in the orbital basis. Since \hat{R} acts on internal degrees of freedom, such as spin or a direction perpendicular to the lattice plane, it acts trivially on the position eigenstates and commutes with lattice translations $\hat{T}_j|o; r\rangle = |o; r+j\rangle$. The commutation condition is necessary for the validity of Eq.(1). Examples to such symmetries are abundant in low dimensional materials or rod and layer space groups.

While for a symmorphic symmetry \hat{R} commutes with the Hamiltonian, in a nonsymmorphic symmetry \hat{R} only commutes with the Hamiltonian when combined with a fractional translation $\hat{T}_{e/n}$ along a unit cell vector e [10, 19]. The combined action $\hat{R}\hat{T}_{e/n}$ relates different points in the unit cell creating a Wyckoff orbit of multiplicity n that ends shifted by a full lattice translation, $(\hat{R}\hat{T}_{e/n})^n = \hat{T}_e$. This fixes the eigenvalues of the nonsymmorphic symmetry to be $\omega^\nu e^{ik\cdot e/n}$. Note that e is not necessarily a basis vector. Finally, the energy eigenstates find their coefficients conditioned by lattice translation symmetry and the nonsymmorphic symmetry to satisfy

$$\phi_o^{\nu k}(r) = e^{ik\cdot j}\phi_o^{\nu k}(r+j) = \omega^\nu e^{i\frac{k\cdot e}{n}}\rho_{oo'}^*\phi_{o'}^{\nu k}(r+e/n). \quad (3)$$

It is illuminating to first see what (3) implies on the form of the energy eigenstates in real and momentum space. Consider \hat{R} a shift in o by one. We can decompose the position r to be $\tilde{r} - ae/n - j$, where $a = 0, \dots, n-1$. Then \tilde{r} is defined in one fraction of the unit cell. Then,

$$|\psi^{\nu k}\rangle = \sum_{oaj} e^{ik\cdot(\frac{a}{n}e+j)}\omega^{\nu a} \int_{\tilde{r}} \phi_o^{\nu k}(\tilde{r})|o-a; \tilde{r} - \frac{a}{n}e - j\rangle, \quad (4)$$

Here $\phi_o(\tilde{r})$ is fixed by the details of the Hamiltonian which are not symmetry dictated. The relationship between contributions of different orbital and position eigenstates is, on the other hand, fixed by symmetry. We can look at a simple one-dimensional example with $n=2$ and $\rho = \sigma_x$. The band structure, shown Fig.1(a), corresponds to a hopping tight-binding Hamiltonian $H(k) = \sin(k/2)\sigma_x$. With only two bands, there is a perfect locking between the orbital (depicted as upwards and downwards droplets) and the atomic position in the unit cell.

Alternatively, in the eigenbasis of \hat{R} (with eigenvalue ω^λ) and momentum $\hat{p} = -i\hat{\partial}_r$ (with eigenvalue p), Eq. (3) is translated to a restriction on the Fourier coefficients of each Bloch state,

$$\bar{\phi}_\lambda^{\nu k}(p) \propto \delta(e^{ip\cdot j} - e^{ik\cdot j})\delta(\omega^\lambda e^{i\frac{a}{n}(p-k)\cdot e} - \omega^\nu). \quad (5)$$

The first δ -function implies momentum is fixed to differ from k by a reciprocal lattice vector G respecting $\exp\{iG\cdot j\} = 1$, which is the essence of Bloch's theorem. Importantly, the

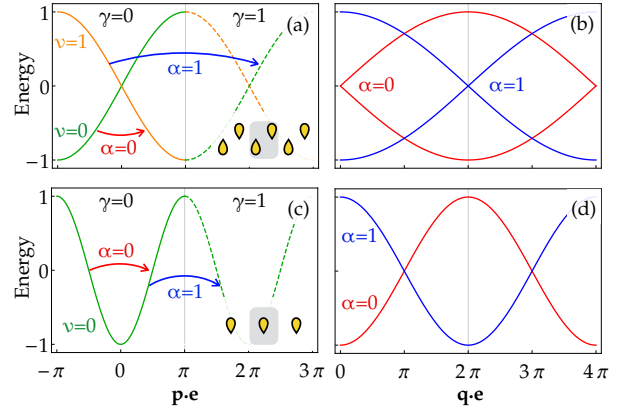


FIG. 1. Scheme of the band structure (a,c) and QPI (b,d) of minimal nonsymmorphic (a,b) and symmorphic (c,d) systems. The values ν , γ and α , determine the selection rules imposed by the operator \hat{m} , according to (1): ν labels the symmetry eigenvalue, γ the BZ along the fractional translation e , and α the difference in γ of the scattered states. In the nonsymmorphic case, α is selected according to the tip character β (9).

second δ -function implies that G fixes the eigenvalue of R , λ . In the diagonal basis, $|\lambda; p\rangle$ then

$$|\psi^{\nu k}\rangle = \sum_G \bar{\phi}_{\nu-\gamma}^{\nu k}(k+G)|\nu-\gamma; k+G\rangle, \quad (6)$$

where we define the shorthand $\gamma \equiv G \cdot e/2\pi \bmod n$.

Note that each Bloch component in (6) is characterized by a different point group eigenvalue. From this it follows how bands with different ν 's meet at the boundaries of the BZ: Changing smoothly $k \rightarrow k+G\cdot e$ implies that both γ and ν shift by an integer after the cycle in opposite ways such that $\nu-\gamma$ is unchanged. That is, there is an adiabatic connection between states of different ν at the boundaries of the BZ, which leads to enforced band crossings (located at the BZ boundary if time-reversal is present) and justifies the large number of degeneracies seen in nonsymmorphic materials [8, 20, 21].

Quasiparticle interference — QPI is a direct measurement of the elastic scattering due to dilute impurities. It is ideal to study symmetry allowed scattering, and it has been extensively used to study topological insulators [22–27], Graphene [28, 29], and high temperature superconductors [17, 30–34]. An impurity located at r_0 that creates (for example) a Gaussian-shaped potential $v(r, r_0) \propto \exp\{-\frac{1}{2}|r-r_0|^2/\xi^2\}$, adds the operator $\hat{V} = \int_r v(r, r_0)|r\rangle\langle r|$, where \hat{v} acts on the \hat{R} subspace, to the electron's Hamiltonian. It is generally not diagonal, and assumed to be random. The tunneling tip can be similarly described by $\hat{M}(r) = |r\rangle\hat{m}\langle r|$, where \hat{m} contains the tunneling elements in orbital space. Finally, in the limit of dilute and weak impurities [23] the measured local density of states is captured by $N(r) = -\text{im} \Lambda(r)/\pi$ with

$$\Lambda(r) = \text{Tr} \hat{M}(r)\mathcal{G}\hat{V}\mathcal{G}, \quad (7)$$

where \mathcal{G} is the retarded (unperturbed) Green's function, and

the trace is taken over the quantum numbers ν and k . Performing a Fourier transformation we write $\hat{M}(\mathbf{q}) = \int_{\mathbf{p}} |\mathbf{p}\rangle \hat{m} \langle \mathbf{p} - \mathbf{q}|$, and $\hat{V} = \int_{\mathbf{p}, \mathbf{q}} v(\mathbf{q}, r_0) |\mathbf{p}\rangle \hat{v} \langle \mathbf{p} - \mathbf{q}|$. The phase associated with the impurity position remains as an overall prefactor, as addressed in Ref. [35]. As we show in the supplementary material [36], the block diagonalization of the eigenstates (6), and the consequent diagonalization of \mathcal{G} , implies that in Fourier space $\Lambda(\mathbf{q})$ can be decomposed in a sum of contributions of the form

$$\Lambda_{kk', \gamma}^{\nu\nu'}(\mathbf{q}, \mathbf{Q}) = \mathcal{I}_{kk', \gamma}^{\nu\nu'}(\mathbf{q}, \mathbf{Q}) \hat{m}_{\nu-\gamma}^{\nu'-\gamma-\alpha} \delta(\mathbf{q} - \mathbf{k}' + \mathbf{k} + \mathbf{Q}), \quad (8)$$

with $\alpha \equiv \mathbf{Q} \cdot \mathbf{e}/2\pi \text{ mod } n$. Each summand in (8) describes the interference of incoming and outgoing waves, weighted by a nonuniversal intensity function \mathcal{I} . The lattice periodicity determines that all processes satisfy $\mathbf{q} - \mathbf{k}' + \mathbf{k} = \mathbf{Q}$, with \mathbf{Q} a reciprocal lattice vector, fixed by the restriction of \mathbf{k} and \mathbf{k}' to the first BZ. Symmetries within the unit cell impose further conditions, and suppress contributions to the QPI as encoded in the matrix elements of \hat{m} . In the nonsymmorphic case, these suppressed contributions depend on \mathbf{Q} . More precisely they depend on α , since it indicates whether momentum is transferred along \mathbf{e} , see Fig. 1.

The function \mathcal{I} , whose explicit form is given in the supplementary material, includes the nonuniversal details that modulate the intensity of the QPI signal. Those include features associated with the impurity, which is only a tool in the experiment, and features associated with the Bloch coefficients, that are dependent on the non symmetry dictated details of the Hamiltonian. The former include the impurity matrix elements, spatial distribution and energy dependence. The exact form of the potential exerted by the impurity may limit the visibility of certain features of the interfering wavefunctions. The latter is determined by the charge distribution within the unit cell. Generally, the first Bloch component is favored and $\alpha = 0$ dominates the QPI, but frequently other values of α are observed as well.

We now focus on what the matrix elements of \hat{m} can tell us about the symmetry dictated features of the interfering electrons, both in the symmorphic and non-symmorphic cases. In the symmorphic case the matrix element in (8) is substituted by $\hat{m}_{\nu'}^{\nu}$. This implies that Eq.(1) is satisfied with $\alpha = 0$, provided the \hat{m} respects

$$\hat{m} \hat{R} = \omega^\beta \hat{R} \hat{m}, \quad (9)$$

If, for example, \hat{m} is diagonal in the eigenspace of \hat{R} , the QPI will manifest only scattering between states of equal eigenvalue ν . This is relevant, for example, in the study of surface states of topological insulators [23, 24], where ν relates to spin, and β to the polarization of a magnetic tunneling tip. In contrast is the nonsymmorphic case, due to the correlation between the amplitude of the momentum $\mathbf{k} + \mathbf{G}$ in the interfering Bloch states and the quantum state of the intracell degrees of freedom. The observed channels satisfy Eq.(1), which allows

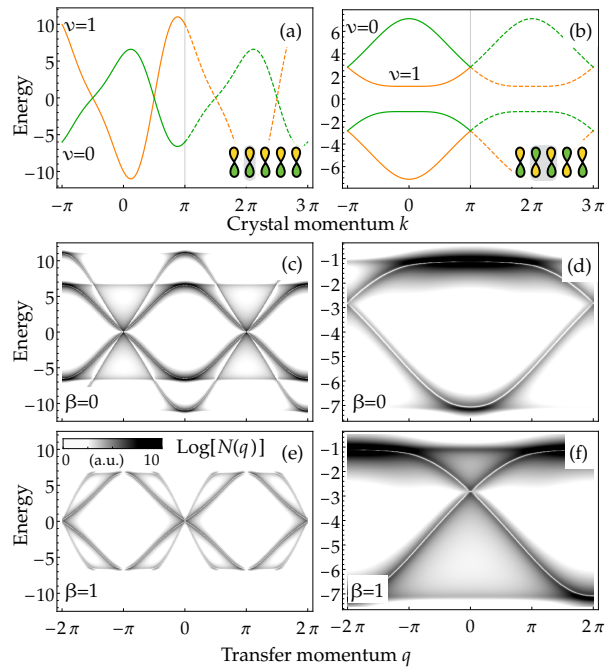


FIG. 2. QPI created by a symmorphic (left) and nonsymmorphic (right) one-dimensional semimetal defined in [36]. (a,b) Band structure, (c-f) QPI, $\text{Log}|N(q)|$ for two distinct measurements $\beta = 0, 1$. The QPI obeys the selection rule: (c) Only scattering within same ν , with a $q = \pi$ crossing of QPI replications, no evidence of Dirac point; (e) Only scattering for different ν , green to orange, with $q = 0, 2\pi$ crossings due to the Dirac points; (d,f) Elastic scattering implies $\nu = \nu'$, thus β selects $\alpha = 1$ in (d) and $\alpha = 0$ in (f). Note that the two replications appear at different β , and there is no crossing at π .

for all scattering channels at all β . However, different channels are manifested at different replications, that is, at different α . In Fig. 1(b) the two replicated signals will be subject to distinct matrix element effects, and thus strongly vary in intensity.

Even though a general measurement will consist of a superposition of β and will generally not be able to fully suppress replications, the relative intensity of different α contains information about the band representations. There are two ways of retrieving this information. First, in the presence of internal nonsymmorphic symmetries matrix elements will alternate along \mathbf{Q}_e . If the impurity is sharply localized, allowing for the observation of many replications, the alternating intensity of QPI peaks along a preferred direction is a strong indicator of a nonsymmorphic structure. Second, β can be used as a tuning knob, varying the intensity of different α channels. Experimentally, this can be achieved by combining data of distinct measurements around an impurity, differing in the tip's position within the unit cell. Since all Hermitian operators can be decomposed as a sum of operators satisfying (9), combining distinct measurements can be used to isolate β . To clarify the latter proposal consider the idealized example presented in Fig.2 (b-inset), with $\rho = \sigma_x$ in the orbital basis. Measuring

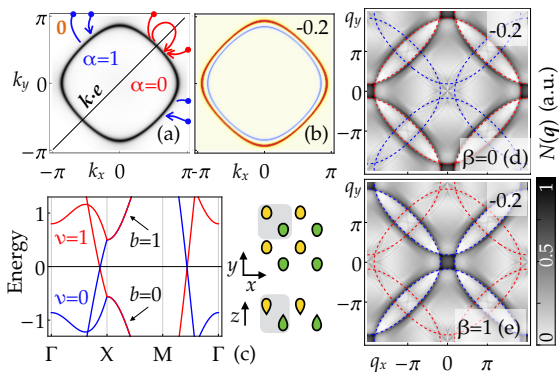


FIG. 3. QPI for an effective model of ZrSiS, with an inplane glide symmetry: (a) Density of states at the Fermi level, marked with scattering processes if different α ; (b) Density of states below the Fermi level, colored by ν . (c) Band structure. (d-e) QPI for the $b = 0$ band at $E = -0.2$. The dashed lines (blue and red) guide the eye to the contributions from different α . The selection rule (1) results in the complete suppression of one α QPI channel, and a remarkable qualitative change in the pattern due to the internal glide symmetry.

a single orbital is represented by $m_{\pm} = \sigma_0 \pm \sigma_z$. Then m_{β} can be constructed by $m_0 = m_+ + m_-$ and $m_1 = m_+ - m_-$. Realistically, a fine tuned superposition is needed, but we note that intracell spatial resolution has been successfully used to highlight surface states in TaAs [37–39].

Numerical simulations — We calculate the QPI numerically for two one-dimensional systems: one symmorphic and one nonsymmorphic and a two-dimensional nonsymmorphic semimetal corresponding to an effective model of ZrSiS [40, 41]. The tight-binding models are given in [36]. In all cases $\omega = -1$. In three dimensions, these can be applied to rod and layer groups.

First, we look at Fig.2. In the symmorphic case (panels a, c and e), we show a two-orbital model with first and second neighbour hopping. The two bands, which carry different eigenvalues of \hat{R} , cross forming two distinct Dirac points in the BZ. The QPI (panels c and e) depends crucially on \hat{n} as expected from (1) but α plays no role. This implies that the crossing of replications at $q = \pi$ is only present in panel (c), and the Dirac points can only be seen in panel (e) at both $q = 0$ and $q = 2\pi$. For the nonsymmorphic chain (b, d and f) we consider a four-band model, with two orbitals at each site. We show the QPI for the two lower energy bands. In contrast with the symmorphic case, here β defines which α signal is observed. This is an evidence for the locking between momentum and \hat{R} eigenvalues. We find in panels (d) and (f) only two lines, and not four. The crossing at $q = \pi$ in (d) is absent, and the evidence for the Dirac point appears only either at $q = 0$ (d) or at $q = 2\pi$ (f) but not both. A Dirac point with equal ν is typical at the boundaries of the BZ in time-reversal symmetric nonsymmorphic systems. Now we consider the two-dimensional model in Fig.3. It can be generally applied to layered nonsymmorphic materials with a glide plane along the surface, with $\mathbf{e} = \hat{x} + \hat{y}$. The relevant physics is well de-

scribed by a four-band model, with two sets of bands, $b = 0, 1$, distinguished by a symmorphic symmetry, protecting a Dirac ring at the Fermi level. The nonsymmorphic symmetry acts on each set separately. Since we are interested in the scattering selection rules for different ν , we choose to show the QPI of a single set $b = 0$. Physically, different bands can occupy different regions in the unit cell, and the impurity position can induce scattering primarily in one set. Consequently, the results are blind to the Dirac ring. We show the density of states (panels a-b) at constant energy resolved by ν , and the QPI (d-e) for $\beta = 0, 1$. The selection rule (1) imposes drastic qualitative differences in the QPI for the different measurements by selecting different α (red and blue dashed lines).

Application to TaAs — In Refs.[37, 38], Batabyal, *et.al.* and Inoue *et.al.* studied the surface QPI of the Weyl semimetal TaAs, focusing on highlighting its arc states. Apart from arc states, both works study additional states, coined “bowtie” and “cigar” surface states, which show Q replications. These results are platform to test our predictions. The intensity modulations of the replications are highly anisotropic: They alternate along Q_y but not along Q_x . From our theory, we propose these modulations reveal a (possibly approximate) nonsymmorphic structure of these surface states. Data in Ref.[38] further indicates that it predominantly occurs at Ta sites. We have verified this prediction by computing the charge density of the “bowtie” state, shown in the supplementary material [36]. Similar analysis of the intensity of replications can be used to detect an onset of a correlated order-parameter that leads to an increase of the unit cell, such as in antiferromagnets.

Conclusion — In this letter we propose a set of measurement-based selection rules to explore the symmetry aspects of Bloch electrons with STM. We do so by expressing the Green’s function in eigenstates of the point-group and momentum operators. When a nonsymmorphic symmetry is present, this decomposition must be performed at each Bloch component of the energy eigenstates independently. We show that two factors are crucial to define universal selection rules. First, how the tunneling tip couples with the local orbital degrees of freedom (β). Second, whether the momentum transfer between energy eigenstates crosses the boundaries of the BZ along the direction of the fractional translation (α). The two factors play an analogous role, evident in Eq. (1) and in the similarity of Figs. 2 (d) and (f). Independently of the impurity potential, we show that the relative intensity of QPI replication of different α , contains information about the symmetry representation of Bloch bands and can be revealed by data analysis. That is, to find a signature of internal nonsymmorphic symmetries we should compare QPI peaks of different Brillouin zones. We further propose that in order to overcome measuring limitations imposed by the finite extent of the atomic orbitals and impurities, we can alternatively explore the spatial resolution of STM. Performing distinct measurements around the same impurity, thereby varying the tunneling elements in orbital space, it is possible to select the tip character β . If the symmetry is nonsymmorphic the two ap-

proaches yield similar results.

The authors acknowledge fruitful discussions with A. Rost, L. Muechler, E. Khalaf; N. Morali, B. Yan, N. Avraham and H. Beidenkopf for pointing out unexplained features in the QPI of TaAs, and B. Yan and H. Fu for calculating the charge density of its surface states. This work was supported by the Israel Science Foundation; the European Research Council under the Project MUNATOP; the DFG (CRC/Transregio 183, EI 519/7-1).

* raquel.queiroz@weizmann.ac.il

† adiel.stern@weizmann.ac.il

- [1] M. S. Dresselhaus, G. Dresselhaus, and A. Jorio, *Group theory* (2008).
- [2] C. Bradley and A. Cracknell, *The mathematical theory of symmetry in solids: representation theory for point groups and space groups* (2010).
- [3] B. Bradlyn, L. Elcoro, J. Cano, M. Vergniory, Z. Wang, C. Felser, M. Aroyo, and B. Bernevig, *Nature* **547**, 298 (2017).
- [4] J. Kruthoff, J. d. Boer, J. v. Wezel, C. L. Kane, and R.-J. Slager, *Physical Review X* **7**, 041069 (2017).
- [5] H. C. Po, A. Vishwanath, and H. Watanabe, *Nature Communications* **8**, 50 (2017).
- [6] C. Herring, *Phys Rev* **52**, 365 (1937).
- [7] J. Zak, *Phys Rev B* **26**, 3010 (1982).
- [8] S. M. Young and C. L. Kane, *Phys Rev Lett* **115**, 126803 (2015).
- [9] H. Po, H. Watanabe, M. P. Zaletel, and A. Vishwanath, *Sci Adv* **2**, e1501782 (2016).
- [10] A. Alexandradinata, Z. Wang, and A. B. Bernevig, *Phys Rev X* **6**, 021008 (2016).
- [11] B. Bradlyn, J. Cano, Z. Wang, M. Vergniory, C. Felser, R. Cava, and B. Bernevig, *Science* **353**, aaf5037 (2016).
- [12] T. Wehling, B. A.M., and A. Balatsky, *Adv Phys* **63**, 1 (2014).
- [13] J. Ma, C. Yi, B. Lv, Z. Wang, S. Nie, L. Wang, L. Kong, Y. Huang, P. Richard, P. Zhang, K. Yaji, K. Kuroda, S. Shin, H. Weng, B. Bernevig, Y. Shi, T. Qian, and H. Ding, **3**, e1602415 (2017).
- [14] M. Crommie, C. Lutz, and D. Eigler, *Nature* **363**, 363524a0 (1993).
- [15] L. Petersen, P. Sprunger, P. Hofmann, E. Lægsgaard, B. Briner, M. Doering, P. H. Rust, A. Bradshaw, F. Besenbacher, and E. Plummer, *Phys Rev B* **57**, R6858 (1998).
- [16] L. Capriotti, D. Scalapino, and R. Sedgewick, *Phys Rev B* **68**, 014508 (2003).
- [17] T. Pereg-Barnea and M. Franz, *Phys Rev B* **68**, 180506 (2003).
- [18] Q. Wang and D. Lee, *Phys Rev B* **67**, 020511 (2003).
- [19] H. Hiller, *Am Math Mon* **93**, 765 (1986).
- [20] Y. Zhao and A. P. Schnyder, *Phys Rev B* **94** (2016).
- [21] S. Young, S. Zaheer, J. Teo, C. Kane, E. Mele, and A. Rappe, *Phys Rev Lett* **108**, 140405 (2012).
- [22] X. Zhou, C. Fang, W. Tsai, and J. Hu, *Phys Rev B* **80** (2009).
- [23] M. H. Guo and M. Franz, *Phys Rev B* **81** (2010), 10.1103/PhysRevB.81.041102.
- [24] J. S. Hofmann, R. Queiroz, and A. P. Schnyder, *Phys Rev B* **88**, 134505 (2013).
- [25] P. Roushan, J. Seo, C. V. Parker, Y. Hor, D. Hsieh, D. Qian, A. Richardella, M. Hasan, R. Cava, and A. Yazdani, *Nature* **460**, 1106 (2009).
- [26] H. Beidenkopf, P. Roushan, J. Seo, L. Gorman, I. Drozdov, Y. Hor, R. Cava, and A. Yazdani, *Nat Phys* **7**, 939 (2011).
- [27] Z. Alpichshev, J. Analytis, J. Chu, I. Fisher, Y. Chen, Z. Shen, A. Fang, and A. Kapitulnik, *Phys Rev Lett* **104**, 016401 (2010).
- [28] G. Rutter, J. Crain, N. Guisinger, T. Li, P. First, and J. Stroscio, *Science* **317**, 219 (2007).
- [29] T. Pereg-Barnea and A. MacDonald, *Phys Rev B* **78**, 014201 (2008).
- [30] J. Hoffman, M. K. D. Lee, K. Lang, H. Eisaki, S. Uchida, and J. Davis, *Science* **297**, 1148 (2002).
- [31] J. Hoffman, E. Hudson, K. Lang, V. Madhavan, H. Eisaki, S. Uchida, and J. Davis, *Science* **295**, 466 (2002).
- [32] T. Hanaguri, S. Niitaka, K. Kuroki, and H. Takagi, *Science* **328**, 474 (2010).
- [33] D. Podolsky, E. Demler, K. Damle, and B. I. Halperin, *Physical Review B* **67**, 094514 (2003).
- [34] K. Fujita, M. H. Hamidian, S. D. Edkins, C. K. Kim, Y. Kohsaka, M. Azuma, M. Takano, H. Takagi, H. Eisaki, S.-i. Uchida, A. Allais, M. J. Lawler, E.-A. Kim, S. Sachdev, and J. C. S. Davis, *Proceedings of the National Academy of Sciences* **111**, E3026 (2014).
- [35] E. G. D. Torre, Y. He, and E. Demler, *Nature Physics* **12**, 1052 (2016).
- [36] See Supplemental Material at <http://link.aps.org/supplemental/10.1103/PhysRevLett.121.176401> for a derivation of the QPI amplitude, the models used in the numerical calculations and an application of this analysis to the QPI pattern of TaAs.
- [37] R. Batabyal, N. Morali, N. Avraham, Y. Sun, M. Schmidt, C. Felser, A. Stern, B. Yan, and H. Beidenkopf, *Sci Adv* **2**, e1600709 (2016).
- [38] H. Inoue, A. Gyenis, Z. Wang, J. Li, S. Oh, S. Jiang, N. Ni, A. B. Bernevig, and A. Yazdani, *Science* **351**, 1184 (2016).
- [39] A. Gyenis, H. Inoue, S. Jeon, B. B. Zhou, B. E. Feldman, Z. Wang, J. Li, S. Jiang, Q. D. Gibson, S. K. Kushwaha, J. W. Krizan, N. Ni, R. J. Cava, A. B. Bernevig, and A. Yazdani, *New J Phys* **18**, 105003 (2016).
- [40] A. Topp, R. Queiroz, A. Grüneis, L. Muechler, A. W. Rost, A. Varykhalov, D. Marchenko, M. Krivenkov, F. Rodolakis, J. L. McChesney, B. V. Lotsch, L. M. Schoop, and C. R. Ast, *Phys. Rev. X* **7**, 041073 (2017).
- [41] L. M. Schoop, M. N. Ali, C. Straßer, A. Topp, A. Varykhalov, D. Marchenko, V. Duppel, S. S. Parkin, B. V. Lotsch, and C. R. Ast, *Nat Commun* **7**, ncomms11696 (2016).

**SUPPLEMENTARY MATERIAL FOR
SELECTION RULES FOR QUASIPARTICLE INTERFERENCE WITH INTERNAL NONSYMMORPHIC SYMMETRIES**

DERIVATION OF THE QUASIPARTICLE INTERFERENCE AMPLITUDE

To analyze the quasiparticle interference pattern, as well as other physical responses, it is convenient to block diagonalize the the Green's function with respect to the crystal momentum \mathbf{k} and symmetry flavor ν ,

$$\mathcal{G}_b^{\nu\mathbf{k}}(E) = \frac{|\psi_b^{\nu\mathbf{k}}\rangle\langle\psi_b^{\nu\mathbf{k}}|}{(E - i0^+) - \varepsilon_b^{\nu\mathbf{k}}} \quad (10)$$

Here $\varepsilon_b^{\nu\mathbf{k}}$ is the band energy, and we omit the explicit dependence in energy, E , to avoid cluttering. Using the eigenstate decomposition in the main text, Eq.6, we find,

$$\mathcal{G}^{\nu\mathbf{k}} = \sum_{\mathbf{G}\mathbf{G}'} |\nu - \gamma; \mathbf{k} + \mathbf{G}\rangle I^{\nu\mathbf{k}}(\mathbf{G}, \mathbf{G}') |\nu - \gamma'; \mathbf{k} + \mathbf{G}'\rangle, \quad (11)$$

where $\gamma = m\mathbf{G} \cdot \mathbf{e}/2\pi \bmod n$ and \mathbf{G} is a reciprocal lattice vector. The relative intensity of each Bloch component takes the explicit form

$$I^{\nu\mathbf{k}}(\mathbf{G}, \mathbf{G}') = \sum_b \frac{\bar{\phi}_{\nu-\gamma}^b(\mathbf{k} + \mathbf{G}) \bar{\phi}_{\nu-\gamma'}^{b*}(\mathbf{k} + \mathbf{G}')}{(E - i0^+) - \varepsilon_b^{\nu\mathbf{k}}}. \quad (12)$$

While the divergence from the denominator only depends on \mathbf{k} , $I^{\nu\mathbf{k}}(\mathbf{G}, \mathbf{G}')$ exponentially decays with \mathbf{G} as a consequence of the spatial width of the atomic wavefunctions.

We calculate the quasiparticle interference amplitude by Fourier transforming the local density of states, which is given by

$$N(\mathbf{r}) = -\frac{1}{\pi} \text{im} \Lambda(\mathbf{r}), \quad \Lambda(\mathbf{r}) = \text{Tr} \hat{M}(\mathbf{r}) \mathcal{G} \hat{V} \mathcal{G}, \quad (13)$$

where the trace is taken over the internal degrees of freedom of the energy eigenstates ν and \mathbf{k} . In Fourier space it is translated to

$$N(\mathbf{q}) = \frac{1}{2\pi i} \{\Lambda^*(-\mathbf{q}) - \Lambda(\mathbf{q})\}, \quad \Lambda(\mathbf{q}) = \text{Tr} \hat{M}(\mathbf{q}) \mathcal{G} \hat{V} \mathcal{G}. \quad (14)$$

Substituting in (14) the tip and impurity operators

$$\hat{M}(\mathbf{q}) = \int_{\mathbf{p}} |\lambda; \mathbf{p}\rangle \hat{m}_{\lambda}^{\lambda'} \langle \lambda'; \mathbf{p} - \mathbf{q}|, \quad \hat{V} = \int_{\mathbf{p}, \mathbf{q}} v(\mathbf{q}, r_0) |\lambda; \mathbf{p}\rangle \hat{v}_{\lambda}^{\lambda'} \langle \lambda'; \mathbf{p} - \mathbf{q}|, \quad (15)$$

as well as the diagonalized Green's function (11), we find that the QPI amplitude decomposes in

$$\Lambda(\mathbf{q}) = \sum_{\nu, \nu', \mathbf{k}, \mathbf{k}'} \sum_{\mathbf{G}, \mathbf{G}', \mathbf{Q}, \mathbf{Q}'} v(\mathbf{q} + \mathbf{Q} + \mathbf{Q}', r_0) I^{\nu\mathbf{k}}(\mathbf{G}, \mathbf{G}') I^{\nu'\mathbf{k}'}(\mathbf{G} + \mathbf{Q}, \mathbf{G}' + \mathbf{Q}') \hat{m}_{\nu-\gamma}^{\nu'-\gamma-\alpha} \hat{v}_{\nu'-\gamma'}^{\nu-\gamma'-\alpha'} \delta(\mathbf{q} - \mathbf{k}' + \mathbf{k} + \mathbf{Q}), \quad (16)$$

with $\alpha = \mathbf{Q} \cdot \mathbf{e}/2\pi \bmod n$ and $\alpha' = \mathbf{Q}' \cdot \mathbf{e}/2\pi \bmod n$ which dictate whether \mathbf{Q} or \mathbf{Q}' crosses the Brillouin zone boundary along the nonsymmorphic direction \mathbf{e} . The summands in (16) can be combined into

$$\Lambda(\mathbf{q}) = \sum_{\nu, \nu', \mathbf{k}, \mathbf{k}', \mathbf{Q}, \gamma} \Lambda_{\mathbf{k}\mathbf{k}', \gamma}^{\nu\nu'}(\mathbf{q}, \mathbf{Q}), \quad \Lambda_{\mathbf{k}\mathbf{k}', \gamma}^{\nu\nu'}(\mathbf{q}, \mathbf{Q}) = \mathcal{I}_{\mathbf{k}\mathbf{k}', \gamma}^{\nu\nu'}(\mathbf{q}, \mathbf{Q}) \hat{m}_{\nu-\gamma}^{\nu'-\gamma-\alpha} \delta(\mathbf{q} - \mathbf{k}' + \mathbf{k} + \mathbf{Q}), \quad (17)$$

by carrying out the sum over the internal variables

$$\mathcal{I}_{\mathbf{k}\mathbf{k}', \gamma}^{\nu\nu'}(\mathbf{q}, \mathbf{Q}) = \sum_{\mathbf{G}, \mathbf{G}', \mathbf{Q}'} v(\mathbf{q} + \mathbf{Q} + \mathbf{Q}', r_0) \mathcal{I}^{\nu\mathbf{k}}(\mathbf{G}, \mathbf{G}') \mathcal{I}^{\nu'\mathbf{k}'}(\mathbf{G} + \mathbf{Q}, \mathbf{G}' + \mathbf{Q}') \hat{v}_{\nu'-\gamma'}^{\nu-\gamma'-\alpha'} \delta_{\omega\gamma, e^{i\mathbf{G}\cdot\mathbf{e}/n}}. \quad (18)$$

Note that \mathbf{Q} , and consequently α , is fully determined by \mathbf{q} and the crystal momentum \mathbf{k} and \mathbf{k}' , since the latter are only defined in the first Brillouin zone. On the other hand \mathbf{Q}' , and consequently α' , is summed over. This the a key ingredient to factor out the matrix elements of \hat{m} . Once we fix the relation,

$$\hat{m} \hat{R} = \omega^\beta \hat{R} \hat{m} \quad (19)$$

it implies that $\hat{m}_{\lambda'}^{\lambda} = 0$ unless $\omega^{\lambda-\lambda'} = \omega^{\beta}$. This means that $\Lambda_{kk',\gamma}^{\nu\nu'}(\mathbf{q}, \mathbf{Q})$ vanishes unless $\omega^{\nu-\nu'+\alpha} = \omega^{\beta}$, for all γ . This is the selection rule presented in the main text.

We point out that the matrix elements introduced by \hat{v} include α' , not fixed by \mathbf{q} . Therefore, they will not enter in the selection rule for $N(\mathbf{q})$ if the symmetry is nonsymmorphic. If, on the other hand, the symmetry flavor ν is symmorphic, we find that the matrix elements are independent of γ or α . That is, when we decompose the QPI amplitude we find the matrix elements to be independent of the Brillouin zone distance \mathbf{Q} ,

$$\Lambda(\mathbf{q}) = \sum_{\nu,\nu',k,k'} \sum_{\mathbf{Q}} \Lambda_{kk'}^{\nu\nu'}(\mathbf{q}, \mathbf{Q}), \quad \Lambda_{kk'}^{\nu\nu'}(\mathbf{q}, \mathbf{Q}) = \mathcal{I}_{kk'}^{\nu\nu'}(\mathbf{q}, \mathbf{Q}) \hat{m}_{\nu'}^{\nu} \hat{v}_{\nu'}^{\nu} \delta(\mathbf{q} - \mathbf{k}' + \mathbf{k} + \mathbf{Q}), \quad (20)$$

with

$$\mathcal{I}_{kk'}^{\nu\nu'}(\mathbf{q}, \mathbf{Q}) = \sum_{\mathbf{G}, \mathbf{G}', \mathbf{Q}'} v(\mathbf{q} + \mathbf{Q} + \mathbf{Q}', r_0) \mathcal{I}^{\nu k}(\mathbf{G}, \mathbf{G}') \mathcal{I}^{\nu' k'}(\mathbf{G} + \mathbf{Q}, \mathbf{G}' + \mathbf{Q}'). \quad (21)$$

That is, the matrix elements of the impurity factor out and become as relevant as the tip matrix elements. Only for probing symmorphic symmetries the impurity and the tip have an interchangeable role.

Finally, we note that the impurity can be invisible to given bands, and in this way further suppress QPI signals, both in the symmorphic and the nonsymmorphic cases.

NUMERICAL CALCULATIONS

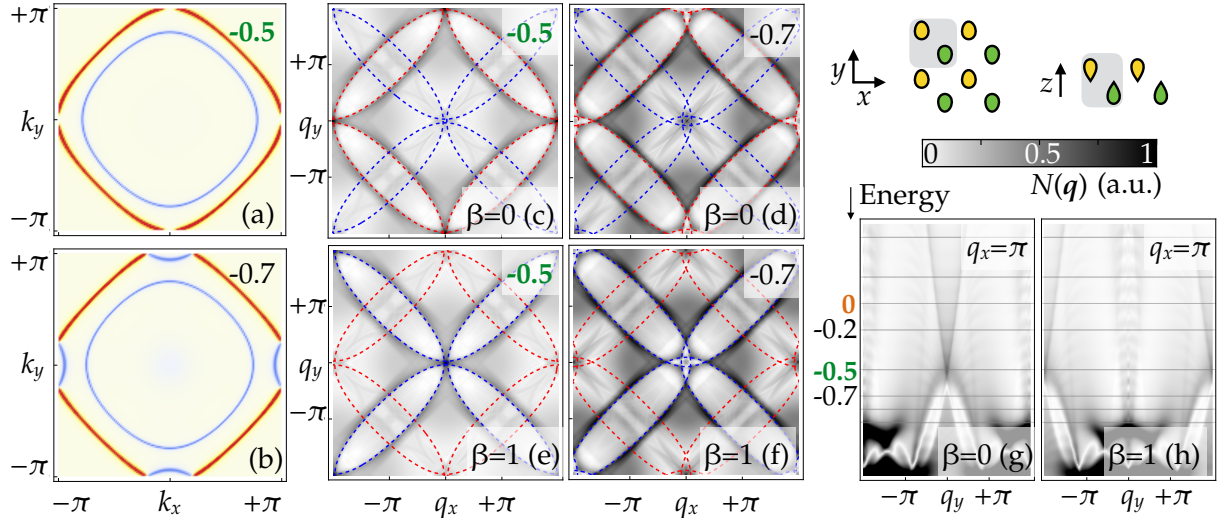


FIG. 4. Additional numerical results for the two-dimensional model. (a,b) Density of states at energies $E = -0.5$ and $E = -0.7$. (c-f) QPI for two measurements with $\beta = 0$ and $\beta = 1$. (g-h) QPI energy cuts with $q_x = \pi$ where the dispersion of the QPI signal can be seen. With $\beta = 0$ we see a crossing at $q_y = 0$ while with $\beta = 1$ the crossing appears at $q_y = \pi$.

In our numerical calculations, we use two one-dimensional models to represent the different phenomenology of a system invariant under a symmorphic and a nonsymmorphic symmetry, both include next nearest neighbour hopping. For a symmorphic chain, we consider

$$H(k) = A_0 + A_1 \cos k + A_2 \cos k \sigma_z + A_3 \sin(2k) + A_4 \sin(2k) \sigma_z, \quad (22)$$

with $A_i = (1, 3, 6, -1/4, 3/4)$. Eq. (22) commutes with σ_z and explicitly breaks time-reversal symmetry. For a nonsymmorphic chain, we consider

$$H(k) = A_0 \sigma_z + A_1 \cos k \sigma_z + A_2 \cos(k/2) \tau_z \sigma_z + A_3 \cos(k/2) \tau_z + A_4 \sin(k/2) \tau_z \sigma_z \quad (23)$$

with $A_i = (3, 1, 2, -1, -1)$. The nonsymmorphic symmetry is given by $e^{ik/2} \tau_z$ and τ_z defines the invariant ν . This model preserves time-reversal symmetry, which pins the crossing of the two bands to the edge of the Brillouin zone. The above models are intended to represent a generic band structure compatible with a symmorphic and a nonsymmorphic symmetry. We do not

discuss the microscopic origin of the different parameters A_i .

In two dimensions we use the model introduced in Ref.[40] to describe the low energy theory of ZrSiS, where the unit cell is composed by two sublattices, shifted by a translation $\mathbf{t} = (\hat{x} + \hat{y})/2$. In an embedded basis, it is given by

$$H(\mathbf{k}) = \mu + m\sigma_z + t_{xy}^{\pm}(\cos k_x + \cos k_y)(1 \pm \sigma_z) + t \cos \frac{k_x}{2} \sin \frac{k_y}{2} \tau_x \quad (24)$$

In the numerical simulations we have used $\mu = 0$, $m = 0.5$, $t_{xy}^- = -t_{xy}^+ = 0.5$, and $t = 2.3$. It is invariant under the nonsymmorphic symmetry $e^{i(k_x+k_y)/2}\tau_x\sigma_z$. The eigenvalues of $\tau_x\sigma_z$ determine ν . The nonsymmorphic symmetry and time-reversal symmetry guarantee that the bands cross at the boundaries of the Brillouin zone.

DIAGNOSING BLOCH SYMMETRY WITH QPI: APPLICATION TO TaAs

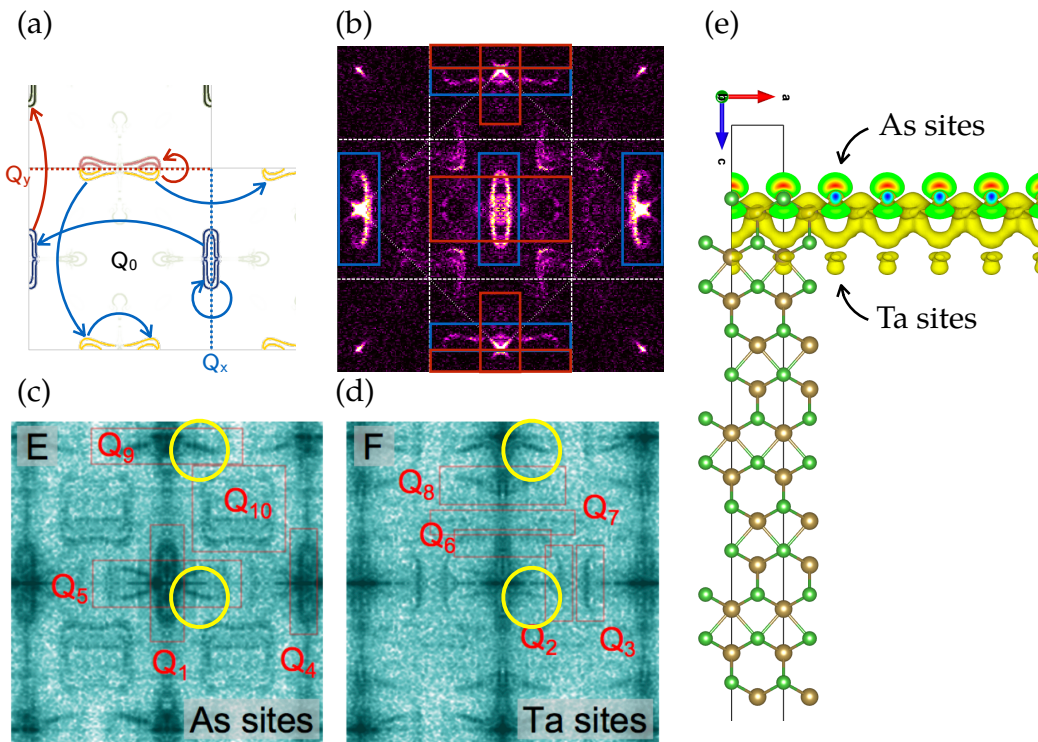


FIG. 5. (a) Adapted from Ref.[37], surface density of states of TaAs, where the “bowtie” and the “cigar” surface states are highlighted. Marked in blue and red arrows are the transitions with a strong and weak intensities in the QPI, respectively. We can identify the weak intensity signal to be associated with momentum transfer of Q_y . (b) From Ref. [37] QPI of surface states of TaAs, where the strong and weak signals are delimited in blue and red boxes, respectively (c-d) From Ref. [38], QPI with atomic resolution, where we have marked in yellow circles the QPI feature of our focus, associated with the “bowtie” state. (c) QPI from As sites where the replications in the x and y direction do not show strong intensity modulations. (d) QPI from Ta sites, the replicated signal in \hat{y} is suppressed, but not in \hat{x} . We can conclude that if this effect comes from matrix elements, it identifies a nonsymmorphic structure along the crystallographic direction a . (e) Density functional theory calculation of the charge density of the “bowtie” surface state. We can distinctly see that contribution of the As sites is symmorphic, while the states around the Ta sites form a zigzag (nonsymmorphic) structure perpendicular to the surface. This calculation was performed by Binghai Yan and Huixia Fu.

* raquel.queiroz@weizmann.ac.il

† adiel.stern@weizmann.ac.il

[1] M. S. Dresselhaus, G. Dresselhaus, and A. Jorio, *Group theory* (2008).

- [2] C. Bradley and A. Cracknell, *The mathematical theory of symmetry in solids: representation theory for point groups and space groups* (2010).
- [3] B. Bradlyn, L. Elcoro, J. Cano, M. Vergniory, Z. Wang, C. Felser, M. Aroyo, and B. Bernevig, *Nature* **547**, 298 (2017).
- [4] J. Kruthoff, J. d. Boer, J. v. Wezel, C. L. Kane, and R.-J. Slager, *Physical Review X* **7**, 041069 (2017).
- [5] H. C. Po, A. Vishwanath, and H. Watanabe, *Nature Communications* **8**, 50 (2017).
- [6] C. Herring, *Phys Rev* **52**, 365 (1937).
- [7] J. Zak, *Phys Rev B* **26**, 3010 (1982).
- [8] S. M. Young and C. L. Kane, *Phys Rev Lett* **115**, 126803 (2015).
- [9] H. Po, H. Watanabe, M. P. Zaletel, and A. Vishwanath, *Sci Adv* **2**, e1501782 (2016).
- [10] A. Alexandradinata, Z. Wang, and A. B. Bernevig, *Phys Rev X* **6**, 021008 (2016).
- [11] B. Bradlyn, J. Cano, Z. Wang, M. Vergniory, C. Felser, R. Cava, and B. Bernevig, *Science* **353**, aaf5037 (2016).
- [12] T. Wehling, B. A.M., and A. Balatsky, *Adv Phys* **63**, 1 (2014).
- [13] J. Ma, C. Yi, B. Lv, Z. Wang, S. Nie, L. Wang, L. Kong, Y. Huang, P. Richard, P. Zhang, K. Yaji, K. Kuroda, S. Shin, H. Weng, B. Bernevig, Y. Shi, T. Qian, and H. Ding, **3**, e1602415 (2017).
- [14] M. Crommie, C. Lutz, and D. Eigler, *Nature* **363**, 363524a0 (1993).
- [15] L. Petersen, P. Sprunger, P. Hofmann, E. Lægsgaard, B. Briner, M. Doering, P. H. Rust, A. Bradshaw, F. Besenbacher, and E. Plummer, *Phys Rev B* **57**, R6858 (1998).
- [16] L. Capriotti, D. Scalapino, and R. Sedgewick, *Phys Rev B* **68**, 014508 (2003).
- [17] T. Pereg-Barnea and M. Franz, *Phys Rev B* **68**, 180506 (2003).
- [18] Q. Wang and D. Lee, *Phys Rev B* **67**, 020511 (2003).
- [19] H. Hiller, *Am Math Mon* **93**, 765 (1986).
- [20] Y. Zhao and A. P. Schnyder, *Phys Rev B* **94** (2016).
- [21] S. Young, S. Zaheer, J. Teo, C. Kane, E. Mele, and A. Rappe, *Phys Rev Lett* **108**, 140405 (2012).
- [22] X. Zhou, C. Fang, W. Tsai, and J. Hu, *Phys Rev B* **80** (2009).
- [23] M. H. Guo and M. Franz, *Phys Rev B* **81** (2010), 10.1103/PhysRevB.81.041102.
- [24] J. S. Hofmann, R. Queiroz, and A. P. Schnyder, *Phys Rev B* **88**, 134505 (2013).
- [25] P. Roushan, J. Seo, C. V. Parker, Y. Hor, D. Hsieh, D. Qian, A. Richardella, M. Hasan, R. Cava, and A. Yazdani, *Nature* **460**, 1106 (2009).
- [26] H. Beidenkopf, P. Roushan, J. Seo, L. Gorman, I. Drozdov, Y. Hor, R. Cava, and A. Yazdani, *Nat Phys* **7**, 939 (2011).
- [27] Z. Alpichshev, J. Analytis, J. Chu, I. Fisher, Y. Chen, Z. Shen, A. Fang, and A. Kapitulnik, *Phys Rev Lett* **104**, 016401 (2010).
- [28] G. Rutter, J. Crain, N. Guisinger, T. Li, P. First, and J. Stroscio, *Science* **317**, 219 (2007).
- [29] T. Pereg-Barnea and A. MacDonald, *Phys Rev B* **78**, 014201 (2008).
- [30] J. Hoffman, M. K. D. Lee, K. Lang, H. Eisaki, S. Uchida, and J. Davis, *Science* **297**, 1148 (2002).
- [31] J. Hoffman, E. Hudson, K. Lang, V. Madhavan, H. Eisaki, S. Uchida, and J. Davis, *Science* **295**, 466 (2002).
- [32] T. Hanaguri, S. Niitaka, K. Kuroki, and H. Takagi, *Science* **328**, 474 (2010).
- [33] D. Podolsky, E. Demler, K. Damle, and B. I. Halperin, *Physical Review B* **67**, 094514 (2003).
- [34] K. Fujita, M. H. Hamidian, S. D. Edkins, C. K. Kim, Y. Kohsaka, M. Azuma, M. Takano, H. Takagi, H. Eisaki, S.-i. Uchida, A. Allais, M. J. Lawler, E.-A. Kim, S. Sachdev, and J. C. S. Davis, *Proceedings of the National Academy of Sciences* **111**, E3026 (2014).
- [35] E. G. D. Torre, Y. He, and E. Demler, *Nature Physics* **12**, 1052 (2016).
- [36] See Supplemental Material at <http://link.aps.org/supplemental/10.1103/PhysRevLett.121.176401> for a derivation of the QPI amplitude, the models used in the numerical calculations and an application of this analysis to the QPI pattern of TaAs.
- [37] R. Batabyal, N. Morali, N. Avraham, Y. Sun, M. Schmidt, C. Felser, A. Stern, B. Yan, and H. Beidenkopf, *Sci Adv* **2**, e1600709 (2016).
- [38] H. Inoue, A. Gyenis, Z. Wang, J. Li, S. Oh, S. Jiang, N. Ni, A. B. Bernevig, and A. Yazdani, *Science* **351**, 1184 (2016).
- [39] A. Gyenis, H. Inoue, S. Jeon, B. B. Zhou, B. E. Feldman, Z. Wang, J. Li, S. Jiang, Q. D. Gibson, S. K. Kushwaha, J. W. Krizan, N. Ni, R. J. Cava, A. B. Bernevig, and A. Yazdani, *New J Phys* **18**, 105003 (2016).
- [40] A. Topp, R. Queiroz, A. Grüneis, L. Müchler, A. W. Rost, A. Varykhalov, D. Marchenko, M. Krivenkov, F. Rodolakis, J. L. McChesney, B. V. Lotsch, L. M. Schoop, and C. R. Ast, *Phys. Rev. X* **7**, 041073 (2017).
- [41] L. M. Schoop, M. N. Ali, C. Straßer, A. Topp, A. Varykhalov, D. Marchenko, V. Duppel, S. S. Parkin, B. V. Lotsch, and C. R. Ast, *Nat Commun* **7**, ncomms11696 (2016).